Microwave Susceptibility Observation of Interacting Many-Body Andreev States

Editors' Suggestion

Microwave Susceptibility Observation of Interacting Many-Body Andreev States

V. Fatemi,[1,*] P. D. Kurilovich,[1] M. Hays,[1] D. Bouman,[2,3] T. Connolly,[1] S. Diamond,[1] N. E. Frattini,[1] V. D. Kurilovich,[1] P. Krogstrup,[4] J. Nygård,[5] A. Geresdi,[2,3,6] L. I. Glazman,[1] and M. H. Devoret[1,†]

[1]*Departments of Physics and Applied Physics, Yale University, New Haven, Connecticut 06520, USA*
[2]*QuTech and Delft University of Technology, 2600 GA Delft, Netherlands*
[3]*Kavli Institute of Nanoscience, Delft University of Technology, 2600 GA Delft, Netherlands*
[4]*Niels Bohr Institute, University of Copenhagen, Universitetsparken 5, 2100 Copenhagen, Denmark*
[5]*Center for Quantum Devices, Niels Bohr Institute, University of Copenhagen, Universitetsparken 5, 2100 Copenhagen, Denmark*
[6]*Quantum Device Physics Laboratory, Department of Microtechnology and Nanoscience, Chalmers University of Technology, SE 41296 Gothenburg, Sweden*

(Received 17 December 2021; accepted 13 September 2022; published 21 November 2022)

Electrostatic charging affects the many-body spectrum of Andreev states, yet its influence on their microwave properties has not been elucidated. We developed a circuit quantum electrodynamics probe that, in addition to transition spectroscopy, measures the microwave susceptibility of different states of a semiconductor nanowire weak link with a single dominant (spin-degenerate) Andreev level. We found that the microwave susceptibility does not exhibit a particle-hole symmetry, which we qualitatively explain as an influence of Coulomb interaction. Moreover, our state-selective measurement reveals a large, π-phase shifted contribution to the response common to all many-body states which can be interpreted as arising from a phase-dependent continuum in the superconducting density of states.

DOI: 10.1103/PhysRevLett.129.227701

Andreev states are the supercurrent-carrying fermionic modes that govern the electrodynamical response of Josephson devices. In devices hosting only a few transport channels, individual states may become energetically well-separated and thus addressable. This direct access to Andreev states has been leveraged to discover new phenomena in mesoscopic superconductivity and unveil applications such as Andreev qubits [1–7]. These experiments probed the microwave frequency response of discrete Andreev states in different regimes: from a minimal configuration of an atomic point contact with one strongly dispersing Andreev level, to multistate configurations in long nanowire weak links where spin-orbit effects become important.

Our understanding of the microwave frequency electrodynamics involving Andreev states has so far relied on noninteracting pictures focusing on the subgap levels [5,8–10]. While such pictures describe atomic point contacts well [1,2], they have two blind spots for any finite-length weak link. First, charging energy should be present when the electrons experience a nonzero dwell time in the weak link. Yet, to our knowledge, the impact of charging energy on the microwave response of Andreev states has not been investigated. This is in contrast to measurements that have revealed a rich interplay between superconductivity and charging effects in dc transport through quantum dots [11–23]. Second, under the same conditions, the spectral continuum outside the superconducting gap (which we will refer to as "the continuum" for brevity) also contributes to the supercurrent [24–26] and therefore is electrodynamically active in finite-length weak links. However, the dynamics of the continuum have not been isolated from the contributions of the subgap Andreev states. This requires measurements that resolve individual many-body configurations of the system.

Are charging effects and the continuum relevant for the microwave response of superconductor-semiconductor weak links? Here, we answer affirmatively by performing state-resolved microwave response measurements with a circuit quantum electrodynamics (CQED) probe. Application of CQED techniques has revealed different quasiparticle occupation configurations of Andreev levels [2,4,6,7], which is possible because the different states of the quantum system have different electrodynamical susceptibility [27]. However, beyond state determination, the magnitude and dispersion of the response functions of individual states carry a wealth of physical information [10,28–31]. This information complements that of microwave and tunneling spectroscopy which are restricted to transitions between states of the same and opposite parity, respectively.

We measured a Josephson semiconductor nanowire with a single low-energy Andreev level coupled to a superconducting microwave resonator. By measuring in the time domain, we extracted the admittance and transition spectrum of different many-body quasiparticle configurations of this level and found two qualitative differences to the standard theory of a deeply subgap Andreev level [8,25,32–35].

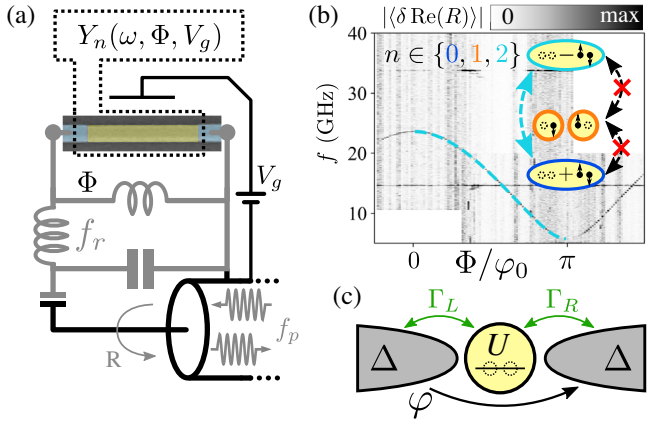

FIG. 1. (a) Schematic of the CQED setup (description in main text), including a colorized scanning electron micrograph of a representative Josephson nanowire weak link (aluminum is dark gray, uncovered region is yellow and 500 nm long in this image, but 350 nm long in the device measured for this report). A probe tone f_p reflects with a frequency-dependent reflection amplitude R which is recorded to measure the system. (b) Two-tone spectroscopy as a function of drive frequency and phase bias revealed a single dispersing Andreev transition, with model fit (dashed cyan line, see Fig. 2 for parameters) corresponding to the transition between the even parity states (inset schematic describes the allowed transitions between the many-body eigenstates within the quantum dot model). Parity-switching transitions are forbidden (black arrows with red X). $n \in \{0, 1, 2\}$ label the eigenstates. The horizontal lines near 15 and 34 GHz are higher harmonics of the resonator. (c) Schematic of our phenomenological model for the lowest level of the weak link: a single-level quantum dot with charging energy U coupled to superconducting reservoirs with gap Δ and phase drop φ [36].

First, the microwave response functions of the even-parity states are not symmetric about the odd state, which we refer to as a violation of a particle-hole symmetry. Second, all states exhibit a common π-shifted contribution to their phase dispersion. We interpret these observations as the qualitative effects of a charging energy in the weak link and phase-dispersing high-energy states, respectively. Our recently developed minimal theory [36] can account for these discrepancies, indicating that the continuum may produce the necessary π-shifted dispersion. Finally, we measured the fermion parity polarization as a function of phase and gate voltage. The switches of the polarization are consistent with 0-π transitions, while the incompleteness of the polarization indicates nonequilibrium parity dynamics. These observations lay a foundation for investigating the interplay of Coulomb interactions with superconducting pairing in conventional and topological superconducting mesoscopic devices with CQED probes.

The salient aspects of our CQED setup are depicted in Fig. 1(a). We grew an indium arsenide nanowire (micrograph) with two facets covered by epitaxial aluminum on which a 350 nm weak-link region was later uncovered. The nanowire weak link is embedded in a superconducting loop that partially determines the inductance of the differential mode of a superconducting microwave resonator (gray). An external coil biased with a dc current inserted magnetic flux Φ through the loop to phase bias the nanowire $\varphi \approx \Phi/\varphi_0$ ($\varphi_0 = \hbar/2e$ is the reduced superconducting magnetic flux quantum). The bare resonator frequency $f_{r,b} = 4.887\,\mathrm{GHz}$ was measured by depleting the weak link with a negative gate voltage V_g.

Discrete Andreev states were introduced to the weak link by opening conduction channels via increasing V_g. While doing this, we conducted two-tone spectroscopy measurements which detect microwave transitions between quantum states of the weak link (this can be seen as probing the dissipative part of the admittance at different frequencies). At low gate voltages, we detected gate "bias points" at which a single dispersing level was identifiable from the spectrum, such as in Fig. 1(b). The discrete transition frequency depends strongly on phase, consistent with a transition between Andreev states at frequency f_A, characterized as the excitation of a pair of localized quasiparticles. In similar microwave experiments, this transition is often compared with the short junction model [1,2,4,37], which requires $f_A = 2\Delta_{\mathrm{Al}}/h$ for $\Phi = 0$. However, the application of this model is inappropriate here since the measured transition frequency is well below twice the gap of the superconducting leads $f_A < 25\ \mathrm{GHz} \ll 2\Delta_{\mathrm{Al}}/h \approx 100\,\mathrm{GHz}$.

Resolution of this discrepancy requires a model that includes a nonzero dwell time for electrons in the weak link. The simplest phenomenological model for this is a quantum dot with a single level coupled to two superconducting leads [15,25,35], schematically shown in Fig. 1(c) [38]. Within this model, dot states with zero and two electrons are hybridized due to the proximity effect between the dot and the leads, parameterized by the tunneling rates $\Gamma_{L,R}$. In the absence of the charging effect ($U = 0$), these states would split symmetrically by $\pm E_A$ with respect to the one-electron state. This splitting leads to the microwave transition frequency $hf_A = 2E_A$. When the proximity effect is weak, the Andreev states formed by this hybridization remain well-detached from the superconducting gap which leads to $f_A \ll 2\Delta_{\mathrm{Al}}/h$ consistent with the experiment. States with a single electron at the dot are also necessarily present in the system. However, when only a single level is accessible, we cannot probe them with two-tone spectroscopy which preserves fermion parity [inset of Fig. 1(b)].

We overcome this limitation with our CQED setup by measuring the discrete frequency shifts of the resonator. This single-tone measurement probes the properties of individual states and minimizes perturbations of the Andreev manifold, distinct from two-tone spectroscopy which intentionally probes the differences between two states by driving transitions. The frequency shifts $\delta f_{r,n}$ are determined by the state-dependent admittance Y_n of

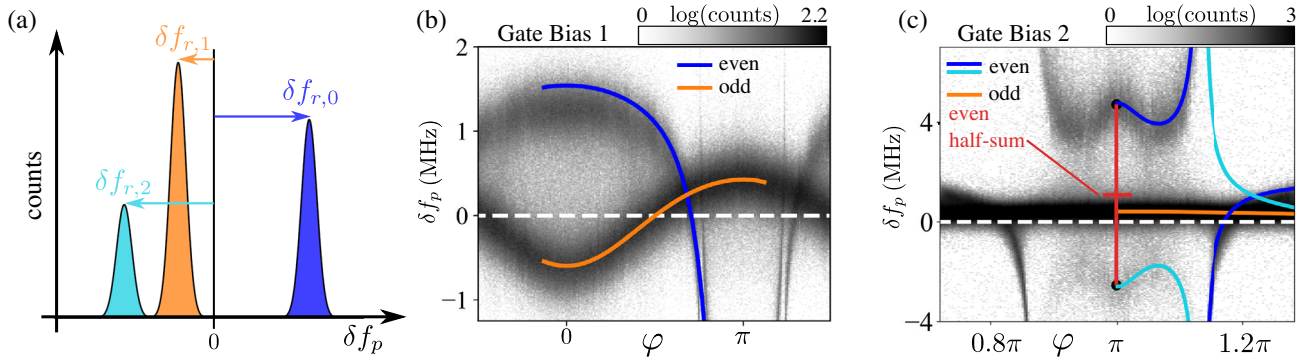

FIG. 2. (a) Schematic of the resonator frequency shift histogram: while sweeping probe frequency relative to the bare resonator frequency $\delta f_p = f_p - f_{r,b}$, we record counts when the reflection signal R indicates a resonance. The magnitude of the frequency shift $\delta f_{r,n}$ is proportional to the admittance Y_n of state n, and normalized counts under each peak give the probability of the state. The widths of the distributions are the same, as they derive from the signal-to-noise ratio of the measurement (see Supplemental Material for details [39]). (b) Resonator frequency shift histogram from the same bias point as Fig. 1(b). Solid lines are model fits of odd (orange) and even (blue) state dispersive shifts $\delta f_{r,n}$ relative to the bare resonator frequency $f_{r,b}$ (white dashed line). The fit parameters in GHz are $\Delta/h = 28.6 \pm 0.3$, $\Gamma_L/h = 6.1 \pm 0.03$, $\Gamma_R/h = 10.4 \pm 0.06$, $U/h = 21.6 \pm 0.8$, and a small offset of $\delta f_{\text{off}} = (0.045 \pm 0.004)$ MHz to the resonator which is 2% of the resonator linewidth of 2 MHz. The small value for Δ may come from a reduced proximity gap or finite-length effects (see Supplemental Material for discussion [39]). (c) Similar to (b) for bias point 2 in a narrow range of phase (see Fig. S8 for a larger phase range). Black circles mark extracted $\delta f_{r,n}$ at $\varphi = \pi$, and the horizontal red bar marks the average of the even-parity frequencies $\frac{1}{2}(\delta f_{r,0} + \delta f_{r,2})$ at $\varphi = \pi$, displaying clear violation of the half-sum rule $\frac{1}{2}(\delta f_{r,0} + \delta f_{r,2}) - \delta f_{r,1} = 0$ (standard deviation is smaller than the red bar thickness). The fit parameters in GHz are $\Delta/h = 25 \pm 6$, $\Gamma_L/h = 7.0 \pm 1.6$, $\Gamma_R/h = 8.1 \pm 1.8$, $U/h = 74 \pm 9$, and $\delta f_{\text{off}} = (1.8 \pm 1.2) \times 10^{-4}$.

the weak link [10,36]: $\delta f_{r,n} \propto \text{Im}[Y_n(2\pi f_{r,b})]$ (see Supplemental Material for more on this [39]). Here n labels the many-body state of the link: $n = 0$, 2 are the two even parity states and $n = 1$ is the spin-degenerate odd state, such that n can be related to the number of quasiparticles in the weak link.

The admittance is given by $Y_n(\omega) = L_n^{-1}/(i\omega) + Y_{n,\text{res}}(\omega)$. The first term describes the quasistatic response of the weak link and is determined by its inverse inductance, $L_n^{-1} = \varphi_0^{-2}\partial_\varphi^2 E_n$. This contribution carries information about the unique energy-phase relations $E_n(\varphi)$ of each microscopic state, which is inaccessible to two-tone spectroscopy. The second term, $Y_{n,\text{res}}(\omega)$, describes the resonant contribution to the admittance and is only appreciable near transition frequencies.

Frequency shift histograms measured as a function of phase are shown for two gate bias points in Figs. 2(b) and 2(c) [50] (details on the overlaid fit curves are given below). Figure 2(b) corresponds to the same bias point as Fig. 1(b). The lowest-energy even state $n = 0$ (blue) is identified by the strong dispersive shift of the resonator when the Andreev pair transition [Fig. 2(b)] approaches the resonator frequency near $\varphi = \pi$. At the second bias point, Fig. 2(c), the Andreev transition crosses the resonator frequency leading to an anticrossinglike feature for the even states. There, the higher-energy even state ($n = 2$) is additionally visible (cyan). At both bias points, an additional state is present in the data. The dispersive shift in this state does not have resonant signatures seen in the even states. We thus identify it as the state with odd fermion parity ($n = 1$).

These measurements exhibit two qualitative discrepancies with the phenomenological dot model in its simplest limit [25,35] of weak coupling to reservoirs and negligible charging energy. First, the odd state $n = 1$ exhibits a strong dispersion in the measurement. In contrast, in the above limit the energies E_n of the states $n \in \{0, 1, 2\}$ can be summarized by

$$E_n = (n - 1)E_A \tag{1}$$

which has $E_1 = 0$. Combined with the lack of transitions, this would result in $\delta f_{r,1} = 0$. Note also that $\delta f_{r,1}$ is π-phase shifted relative to $\delta f_{r,0}$ which excludes a parallel channel interpretation. The second qualitative feature is observed when all three possible occupations $n \in \{0, 1, 2\}$ are observed, as in Fig. 2(c). There, the average frequency shift of the even states (the "half-sum" of $n = 0$, 2) is different from that of the odd state ($n = 1$): $\frac{1}{2}(\delta f_{r,0} + \delta f_{r,2}) - \delta f_{r,1} \approx 0.6$ MHz [51]. This observation is indicated by the red lines and does not require comparison to a model. Conventional noninteracting pictures for Andreev states (like the weak-coupling model described earlier) would predict zero such difference (i.e., the half-sum rule $\frac{1}{2}(\delta f_{r,0} + \delta f_{r,2}) - \delta f_{r,1} = 0$) due to a particle-hole symmetry, as in Eq. (1).

How may we reconcile these two discrepancies? First, the dispersion of the odd state may be accounted for by a phase-dispersing spectral continuum above the gap of the superconductor. The continuum is thus understood to

produce a contribution $E_{\rm cont}$ common to all many-body states $n \in \{0, 1, 2\}$. The presence of the appreciable continuum contribution to energy is a consequence of intermediate-strength tunnel coupling between the dot and the superconducting leads. Second, the half-sum violation suggests that particle-hole symmetry is broken by a charging energy in the weak link. These notions prompt us to qualitatively generalize the prior formulation to

$$E_n = E_{\rm cont} + (n-1)E_A + (n-1)^2 U_A \qquad (2)$$

where U_A is a term related to charging energy that is phase dependent since the Andreev eigenstates are not charge eigenstates. Thus, both experimental discrepancies may be accounted for via inductive contributions to the dispersive shifts following from Eq. (2): $\partial_\varphi^2 E_1 = \partial_\varphi^2 E_{\rm cont}$ and $\frac{1}{2}(\partial_\varphi^2 E_0 + \partial_\varphi^2 E_2) - \partial_\varphi^2 E_1 = \partial_\varphi^2 U_A$.

We compared our data with our recently developed model for a single-level quantum dot coupled to two superconducting reservoirs [36], which we describe in detail in the Supplemental Material [39]. The model includes a Coulomb interaction parameter U perturbatively, assuming $U \ll \Delta + \Gamma$ [36]. At each gate bias point, we performed a least-squares fit to all available dispersive data ($\delta f_{r,n}$ and the transition f_A) simultaneously. The bias points are gate voltage V_g "sweet spots" where the transition frequency was at a minimum, thus minimizing charge noise (see Supplemental Material [39]).

The fitted model is overlaid on the data [Figs. 1(b) and 2(b) for gate bias point 1, Fig. 2(c) for gate bias point 2]. We begin with bias point 1. Remarkably, our simple model quantitatively reproduces the π-phase shifted response of the odd parity state (orange) by including the physics of the continuum. Indeed, for $\Gamma \ll \Delta$, we find $E_{\rm cont} \approx (\Gamma_R \Gamma_L/\Delta)\cos\varphi$, giving rise to the π-shifted behavior of the admittance in the odd state. Deviations from a cosine behavior [apparent in Fig. 2(b) under close inspection] are also well captured by our model in the intermediate-coupling regime $\Gamma \sim \Delta$. The continuum contribution to the even state $n = 0$ is also important: it results in a lower admittance (smaller frequency shift) than would otherwise be expected, an important effect when incorporating such weak links into microwave circuits [30,52,53].

The model also reproduces the violation of the half-sum rule due to the charging energy, as shown in Fig. 2(c). The theory correctly accounts for the sign of the effect $\frac{1}{2}(\delta f_{r,0} + \delta f_{r,2}) > \delta f_{r,1}$. However, the fit in Fig. 2(c) gives $U \gtrsim \Delta + \Gamma$, which is beyond the validity of our perturbative theory (see Fig. 2 caption and [36]). In future Letter, numerical renormalization group methods [54] could be extended to analyze these effects. Nonetheless, our simple model indicates that charging effects in the weak link are appreciable [55].

Charging effects of this strength can overcome superconducting pairing to produce an odd parity ground state.

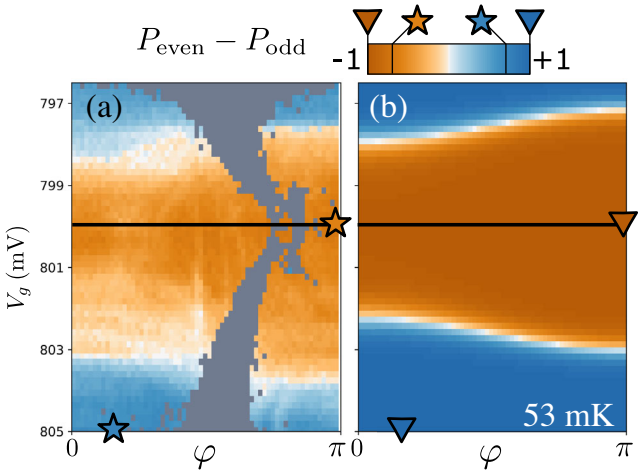

FIG. 3. The difference in the occupation probability of the even $n = 0$ and odd $n = 1$ states $P_{\rm even} - P_{\rm odd}$ (i.e., the fermion parity polarization) as a function of φ and V_g near gate bias point 2. Panel (a) is the experiment and (b) is a thermal equilibrium prediction within our model for the energies. Both panels have the same pixels and color scale. We assume that the energy of the level in the dot is proportional to V_g for simplicity (see Supplemental Material for calibration [39]). (a) Gray regions denote where $\delta f_{r,n}$ were too similar to obtain reliable information. Orange and blue stars indicate the extremal experimental polarizations. (b) We use $T = 53$ mK for the thermal equilibrium prediction (see Supplemental Material for calibration [39]). All other parameters were taken from the fit in Fig. 2(c), which was taken along the black line.

Within the model, the odd state is energetically favored for a range of phase and gate voltage centered at $\varphi = \pi$ and V_g corresponding to the even charge basis state degeneracy, respectively. To check this in the experiment, we quantified the difference in the probability of the fermion parities $P_{\rm even} - P_{\rm odd}$ (the polarization) as a function of phase φ and gate voltage V_g for bias point 2, shown in Fig. 3(a) (see Supplemental Material for details [39]). The sweet spot at $V_g = 800$ mV [same as Fig. 2(c)] exhibits majority-odd population (orange) for all phases. Detuning the gate voltage V_g results in a transition (white) to majority-even (blue). The transition voltage increases when tuning φ from 0 to π, suggestive of a more stable odd state at $\varphi = \pi$. Together, these results are consistent with a 0-π transition for the weak link, as would be expected from the energies of the interacting quantum dot model. To the best of our knowledge, this is the first time that such a phase diagram has been measured in a microwave experiment.

We can compare with the predictions of thermal equilibrium using the state energies predicted by our model, shown Fig. 3(b). We independently calibrated the weak link temperature at 53 mK based on the relative probability of the same-parity states $n = 0, 2$ observed near phase $\varphi = \pi$ (see Supplemental Material [39]). We find a similar pattern for the sign of the polarization as the experiment, but a

difference is evident in the polarization magnitude, indicated by the color darkness. Most of the theoretical phase diagram exhibits full polarization $1 - |P_{\text{even}} - P_{\text{odd}}| \ll 1$ because the typical fermion parity energy difference is much larger than the inferred temperature $|E_0 - E_1|/k_B \gg 53$ mK (k_B is Boltzmann's constant). The experimental weak link, however, never exceeds a polarization of 0.7, which, taken at face value, would require temperature > 500 mK, over an order of magnitude larger than that seen in the even states. Quasiparticles in superconducting devices are known to be out of equilibrium, so parity dynamics may not follow from the expectations of thermodynamic equilibrium [56]. Our data points to the need for a model of nonequilibrium fermion parity dynamics to quantitatively explain the variation of the polarization with phase bias.

In closing, we employed a CQED setup to quantify the microwave response of many-body Andreev states in a superconducting weak link. We identified two important features in the dispersion of the microwave response functions. One is a violation of a particle-hole symmetry resulting from charging effects. The second is a phase dispersion common to all states consistent with the contribution of a spectral continuum. Finally, we observed switches of parity polarization when varying gate voltage and phase bias that are consistent with a 0-π transition.

We would like to acknowledge two other experimental teams pursuing related research on Coulomb interaction in Andreev states. We thank F. J. Matute Canadas, C. Metzger, S. Park, L. Tosi, M. F. Goffman, C. Urbina, H. Pothier, A. Levy-Yeyati for sharing their manuscript [57], for useful comments on ours, and for fruitful discussions. We thank A. Bargerbos, M. Pita-Vidal, R. Zitko, R. Aguado, A. Kou, and B. van Heck for sharing their data [58] and for helpful comments and discussions. We also thank M. Houzet, J. Vayrynen, and L. Bretheau for helpful discussions and L. Frunzio for assistance with device fabrication. This work is supported by the ARO under Grant No. W911NF-18-1-0212. The views and conclusions contained in this document are those of the authors and should not be interpreted as representing the official policies, either expressed or implied, of the Army Research Office (ARO), or the U.S. Government. The U.S. Government is authorized to reproduce and distribute reprints for Government purposes notwithstanding any copyright notation herein. V. D. K. and L. I. G. acknowledge the support of NSF DMR-2002275. D. B. acknowledges support by Netherlands Organisation for Scientific Research (NWO) and Microsoft Corporation Station Q. P. K. acknowledges support from Microsoft Quantum and the European Research Council under the Grant Agreement No. 716655 (HEMs-DAM). J. N. acknowledges support from the Danish National Research Foundation. Some of the authors acknowledge the European Union's Horizon 2020 research and innovation programme for financial support: A. G. received funding from the European Research Council, Grant No. 804988 (SiMS), and A. G. and J. N. further acknowledge Grant No. 828948 (AndQC) and QuantERA Project No. 127900 (SuperTOP). We thank Will Oliver and Lincoln Laboratories for providing the traveling wave parametric amplifier used in this experiment. Facilities use was supported by YINQE and the Yale SEAS cleanroom. We also acknowledge the Yale Quantum Institute. P. K. and J. N. developed the nanowire materials. V. F., M. H., N. F., D. B., S. D., and A. G. designed the experimental setup. V. F., D. B., and S. D. fabricated the nanowire and resonator device. V. F. performed the measurements with feedback from P. D. K., M. H., V. D. K., N. F., and S. D. V. F., P. D. K., V. D. K., M. H., T. C., N. F., S. D., L. I. G., and M. H. D. analyzed the data. V. F., P. D. K., V. D. K., L. I. G., and M. H. D. wrote the manuscript with feedback from all authors.

*valla.fatemi@yale.edu
†michel.devoret@yale.edu

[1] L. Bretheau, Localized excitations in superconducting atomic contacts: Probing the Andreev doublet, thesis, Ecole Polytechnique, 2013.
[2] C. Janvier, L. Tosi, L. Bretheau, C. O. Girit, M. Stern, P. Bertet, P. Joyez, D. Vion, D. Esteve, M. F. Goffman, H. Pothier, and C. Urbina, Science **349**, 1199 (2015).
[3] D. J. van Woerkom, A. Proutski, B. van Heck, D. Bouman, J. I. Väyrynen, L. I. Glazman, P. Krogstrup, J. Nygård, L. P. Kouwenhoven, and A. Geresdi, Nat. Phys. **13**, 876 (2017).
[4] M. Hays, G. de Lange, K. Serniak, D. J. van Woerkom, D. Bouman, P. Krogstrup, J. Nygård, A. Geresdi, and M. H. Devoret, Phys. Rev. Lett. **121**, 047001 (2018).
[5] L. Tosi, C. Metzger, M. F. Goffman, C. Urbina, H. Pothier, S. Park, A. L. Yeyati, J. Nygård, and P. Krogstrup, Phys. Rev. X **9**, 011010 (2019).
[6] M. Hays, V. Fatemi, K. Serniak, D. Bouman, S. Diamond, G. de Lange, P. Krogstrup, J. Nygård, A. Geresdi, and M. H. Devoret, Nat. Phys. **16**, 1103 (2020).
[7] M. Hays, V. Fatemi, D. Bouman, J. Cerrillo, S. Diamond, K. Serniak, T. Connolly, P. Krogstrup, J. Nygård, A. L. Yeyati, A. Geresdi, and M. H. Devoret, Science **373**, 430 (2021).
[8] F. Kos, S. E. Nigg, and L. I. Glazman, Phys. Rev. B **87**, 174521 (2013).
[9] S. Park and A. L. Yeyati, Phys. Rev. B **96**, 125416 (2017).
[10] S. Park, C. Metzger, L. Tosi, M. F. Goffman, C. Urbina, H. Pothier, and A. L. Yeyati, Phys. Rev. Lett. **125**, 077701 (2020).
[11] W. Chang, V. E. Manucharyan, T. S. Jespersen, J. Nygård, and C. M. Marcus, Phys. Rev. Lett. **110**, 217005 (2013).
[12] M. R. Buitelaar, W. Belzig, T. Nussbaumer, B. Babić, C. Bruder, and C. Schönenberger, Phys. Rev. Lett. **91**, 057005 (2003).
[13] J. A. van Dam, Y. V. Nazarov, E. P. A. M. Bakkers, S. De Franceschi, and L. P. Kouwenhoven, Nature (London) **442**, 667 (2006).
[14] H. I. Jorgensen, T. Novotny, K. Grove-Rasmussen, K. Flensberg, and P. E. Lindelof, Nano Lett. **7**, 2441 (2007).

[15] J.-D. Pillet, C. H. L. Quay, P. Morfin, C. Bena, A. L. Yeyati, and P. Joyez, Nat. Phys. **6**, 965 (2010).

[16] S. Li, N. Kang, P. Caroff, and H. Q. Xu, Phys. Rev. B **95**, 014515 (2017).

[17] B.-K. Kim, Y.-H. Ahn, J.-J. Kim, M.-S. Choi, M.-H. Bae, K. Kang, J. S. Lim, R. López, and N. Kim, Phys. Rev. Lett. **110**, 076803 (2013).

[18] E. J. H. Lee, X. Jiang, M. Houzet, R. Aguado, C. M. Lieber, and S. De Franceschi, Nat. Nanotechnol. **9**, 79 (2014).

[19] R. Delagrange, D. J. Luitz, R. Weil, A. Kasumov, V. Meden, H. Bouchiat, and R. Deblock, Phys. Rev. B **91**, 241401(R) (2015).

[20] D. B. Szombati, S. Nadj-Perge, D. Car, S. R. Plissard, E. P. a. M. Bakkers, and L. P. Kouwenhoven, Nat. Phys. **12**, 568 (2016).

[21] E. J. H. Lee, X. Jiang, R. Žitko, R. Aguado, C. M. Lieber, and S. De Franceschi, Phys. Rev. B **95**, 180502(R) (2017).

[22] D. Razmadze, E. C. T. O'Farrell, P. Krogstrup, and C. M. Marcus, Phys. Rev. Lett. **125**, 116803 (2020).

[23] Z. Su, R. Žitko, P. Zhang, H. Wu, D. Car, S. R. Plissard, S. Gazibegovic, G. Badawy, M. Hocevar, J. Chen, E. P. A. M. Bakkers, and S. M. Frolov, Phys. Rev. B **101**, 235315 (2020).

[24] I. Kulik, J. Exp. Theor. Phys. **30**, 944 (1970), http://jetp.ras.ru/cgi-bin/e/index/e/30/5/p944?a=list.

[25] C. W. J. Beenakker and H. v. Houten, in *Single-Electron Tunneling and Mesoscopic Devices*, Springer Series in Electronics and Photonics (Springer, Berlin, Heidelberg, 1992), pp. 175–179.

[26] V. Meden, J. Phys. Condens. Matter **31**, 163001 (2019).

[27] A. Blais, A. L. Grimsmo, S. M. Girvin, and A. Wallraff, Rev. Mod. Phys. **93**, 025005 (2021).

[28] A. Paila, D. Gunnarsson, J. Sarkar, M. A. Sillanpää, and P. J. Hakonen, Phys. Rev. B **80**, 144520 (2009).

[29] D. N. Basov, R. D. Averitt, D. van der Marel, M. Dressel, and K. Haule, Rev. Mod. Phys. **83**, 471 (2011).

[30] C. Metzger, S. Park, L. Tosi, C. Janvier, A. A. Reynoso, M. F. Goffman, C. Urbina, A. Levy Yeyati, and H. Pothier, Phys. Rev. Res. **3**, 013036 (2021).

[31] R. Haller, G. Fülöp, D. Indolese, J. Ridderbos, R. Kraft, L. Y. Cheung, J. H. Ungerer, K. Watanabe, T. Taniguchi, D. Beckmann, R. Danneau, P. Virtanen, and C. Schönenberger, Phys. Rev. Res. **4**, 013198 (2022).

[32] D. A. Ivanov and M. V. Feigel'man, Phys. Rev. B **59**, 8444 (1999).

[33] A. Zazunov, V. S. Shumeiko, E. N. Bratus', J. Lantz, and G. Wendin, Phys. Rev. Lett. **90**, 087003 (2003).

[34] A. Zazunov, V. S. Shumeiko, G. Wendin, and E. N. Bratus', Phys. Rev. B **71**, 214505 (2005).

[35] G. Wendin and V. S. Shumeiko, Superlattices Microstruct. **20**, 569 (1996).

[36] P. D. Kurilovich, V. D. Kurilovich, V. Fatemi, M. H. Devoret, and L. I. Glazman, Phys. Rev. B **104**, 174517 (2021).

[37] D. J. van Woerkom, P. Scarlino, J. H. Ungerer, C. Müller, J. V. Koski, A. J. Landig, C. Reichl, W. Wegscheider, T. Ihn, K. Ensslin, and A. Wallraff, Phys. Rev. X **8**, 041018 (2018).

[38] Models with weak link length of order the coherence length also exhibit dwell time. Such models admit additional doublets and add theoretical complications, see Supplemental Material V.E. [39].

[39] See Supplemental Material at http://link.aps.org/supplemental/10.1103/PhysRevLett.129.227701, which contains device details, fabrication procedure, data analysis methods, theoretical methods and pedagogical content, comparison with a long-junction model, data on nonlinear effects, gate-voltage dependence data, and temperature-dependence analysis [40–49].

[40] N. E. Frattini, U. Vool, S. Shankar, A. Narla, K. M. Sliwa, and M. H. Devoret, Appl. Phys. Lett. **110**, 222603 (2017).

[41] P. Krogstrup, N. L. B. Ziino, W. Chang, S. M. Albrecht, M. H. Madsen, E. Johnson, J. Nygård, C. M. Marcus, and T. S. Jespersen, Nat. Mater. **14**, 400 (2015).

[42] K. Flöhr, M. Liebmann, K. Sladek, H. Y. Günel, R. Frielinghaus, F. Haas, C. Meyer, H. Hardtdegen, T. Schäpers, D. Grützmacher, and M. Morgenstern, Rev. Sci. Instrum. **82**, 113705 (2011).

[43] O. Gul, H. Zhang, F. K. de Vries, J. van Veen, K. Zuo, V. Mourik, S. Conesa-Boj, M. P. Nowak, D. J. van Woerkom, M. Quintero-Perez, M. C. Cassidy, A. Geresdi, S. Koelling, D. Car, S. R. Plissard, E. P. A. M. Bakkers, and L. P. Kouwenhoven, Nano Lett. **17**, 2690 (2017).

[44] J. Krupka, K. Derzakowski, M. Tobar, J. Hartnett, and R. G. Geyer, Meas. Sci. Technol. **10**, 387 (1999).

[45] L. Bretheau, C. O. Girit, H. Pothier, D. Esteve, and C. Urbina, Nature (London) **499**, 312 (2013).

[46] V. Fatemi, P. D. Kurilovich, M. Hays, D. Bouman, T. Connoly, S. Diamond, N. E. Frattini, V. D. Kuriloivch, P. Krogstrup, J. Nygard, A. Geresdi, L. I. Glazman, and M. H. Devoret, Zenodo, 10.5281/zenodo.5682952 (2021), type: dataset.

[47] J. Gambetta, A. Blais, D. I. Schuster, A. Wallraff, L. Frunzio, J. Majer, M. H. Devoret, S. M. Girvin, and R. J. Schoelkopf, Phys. Rev. A **74**, 042318 (2006).

[48] J. R. Johansson, P. D. Nation, and F. Nori, Comput. Phys. Commun. **183**, 1760 (2012).

[49] J. R. Johansson, P. D. Nation, and F. Nori, Comput. Phys. Commun. **184**, 1234 (2013).

[50] Probe tone power corresponding to roughly nine photons in the resonator.

[51] This naïve comparison is in principle susceptible to corrections to the dispersive shifts because they are solutions of a transcendental equation which is inherently nonlinear in $Y(\omega)$ (see Supplemental Material [39]). We estimate the corrections to be less than 10% of the mismatch observed here. Furthermore, our probe power is small enough that frequency shifts due to nonlinearities are minimal.

[52] A. Bargerbos, W. Uilhoorn, C.-K. Yang, P. Krogstrup, L. P. Kouwenhoven, G. de Lange, B. van Heck, and A. Kou, Phys. Rev. Lett. **124**, 246802 (2020).

[53] A. Kringhøj, B. van Heck, T. W. Larsen, O. Erlandsson, D. Sabonis, P. Krogstrup, L. Casparis, K. D. Petersson, and C. M. Marcus, Phys. Rev. Lett. **124**, 246803 (2020).

[54] A. Kadlecová, M. Žonda, V. Pokorný, and T. Novotný, Phys. Rev. Appl. **11**, 044094 (2019).

[55] We note that a naive estimation based on the dimensions of the uncovered weak link region gives of order $U \sim 200$ GHz, whereas our fits produce values of U up to an order of magnitude smaller. This suggests strong screening by the epitaxial aluminum leads.
[56] L. Glazman and G. Catelani, SciPost Phys. Lect. Notes 31 (2021).10.21468/SciPostPhysLectNotes.31
[57] F. J. M. Cañadas, C. Metzger, S. Park, L. Tosi, P. Krogstrup, J. Nygård, M. F. Goffman, C. Urbina, H. Pothier, and A. L. Yeyati, Phys. Rev. Lett. **128**, 197702 (2022).
[58] A. Bargerbos, M. Pita-Vidal, R. Žitko, J. Ávila, L. J. Splitthoff, L. Grünhaupt, J. J. Wesdorp, C. K. Andersen, Y. Liu, L. P. Kouwenhoven, R. Aguado, A. Kou, and B. van Heck, PRX Quantum **3**, 030311 (2022).